Defying Thermodynamics: Stabilization of Alane Within Covalent Triazine Frameworks for Reversible Hydrogen Storage

Vitalie Stavila[1],*§ Sichi Li[2],§ Chaochao Dun,[3] Maxwell A. T. Marple[2], Harris E. Mason[2], Jonathan L. Snider[1], Joseph E. Reynolds III,[1] Catalin Spataru,[1] Xiaowang Zhou,[1] Brennan Dizdar,[4,6] Eric H. Majzoub,[4] Hendrik Schlomberg[5], Bettina V. Lotsch[5], Jeffrey J. Urban,[3] Brandon C. Wood,[2] Mark D. Allendorf[1]*

[1]Sandia National Laboratories, 7011 East Avenue, Livermore, CA 94550, United States

[2]Lawrence Livermore National Laboratory, 7000 East Avenue, Livermore, CA 94550, United States

[3]Lawrence Berkeley National Laboratory, 1 Cyclotron Rd, Berkeley, CA 94720, United States

[4]University of Missouri - St. Louis, Department of Physics and Astronomy, One University Blvd, St. Louis, MO, 63121, United States

[5]Max-Planck-Institut für Festkörperforschung, Heisenbergstraße 1, 70569 Stuttgart, Germany

[6]University of Chicago, Chicago, Illinois 60637, United States

[§] Contributed equally to this work

E-mail: vnstavi@sandia.gov; mdallen@sandia.gov

ABSTRACT: Metastable metal hydrides have many attractive features as hydrogen storage media, but generally cannot be directly regenerated under hydrogen gas and require complex regeneration schemes. Here, we demonstrate nanoconfinement of metastable aluminum hydride inside pores of two Covalent Triazine Frameworks, CTF-bipyridine and CTF-biphenyl. The resulting nanoconfined materials exhibit rapid hydrogen release between 90 and 150 °C, with full desorption into metallic aluminum at 250 °C. Sieverts, ^{27}Al MAS NMR, ^{27}Al{^{1}H} REDOR experiments, coupled with computational spectroscopy, reveal that AlH_3@CTF-bipyridine can be regenerated at 60 °C under 700 bar hydrogen, a pressure which is >10 times lower compared to the pressure required to rehydrogenate bulk metallic Al. In contrast, no reversibility is observed for the AlH_3@CTF-biphenyl material. DFT calculations show that the presence of small AlH_3 clusters, coupled with the efficient charge redistribution between the hydride and bipyridine groups of CTF-bipyridine, is critical to the observed reversibility.

INTRODUCTION

Hydrogen is increasingly viewed as a contemporary solution to world energy problems as it can store surplus renewables power, decarbonize transportation, and replace fossil fuels as a zero-emission energy carrier.[1-2] However, conventional ways to store hydrogen by high-pressure or cryogenic approaches pose significant technical and engineering challenges, and alternative methods, such as solid-state storage, are receiving increased attention.[3] Metal hydrides are particularly promising as H_2 storage media, as they provide high energy densities and can operate near ambient conditions of temperature and pressure.[4-5] Nanoscale metal hydrides display certain advantages compared to bulk,[6] by enhancing the rates of H_2 uptake, destabilizing stable intermediates,[7] and enabling or improving reversibility.[8] Despite successes in accelerating the reaction rates, control over the thermodynamics of chemical processes in nanoscale metal hydrides has not been fully achieved and is poorly understood. Majzoub *et al*. have shown that nanoconfinement of both $LiBH_4$ and $NaAlH_4$ in N-functionalized porous carbons alters the decomposition pathway and activation energy of hydrogen release,[9-10] however the guest-host interactions are rather weak to alter the thermodynamics. Covalent Organic Frameworks (COFs) [11] and Metal Organic Frameworks (MOFs)[12] are alternative platforms for investigating interactions between porous hosts and metal hydrides, as a multitude of pore functionalities exists or can be achieved through post-synthetic modifications.[13] Theoretical and experimental studies using such host materials show a marked increase in the dehydrogenation reaction rates of several binary and complex metal hydrides, in particular when particle sizes are below 10 nm.[14-16]

Here, we demonstrate thermodynamic stabilization of aluminum hydride (AlH_3, alane) confined inside the pores of Covalent Triazine Framework (CTF) materials. Two CTF materials were selected for this study, one containing biphenyl groups, and the other one of similar topology with bipyridine groups (**Scheme 1**). Antonietti, Thomas, and co-workers pioneered the synthesis and applications of CTFs and were the first to report high surface areas in these materials.[17-18] CTFs are synthesized by trimerization of the cyano- groups of aromatic nitriles via ionothermal synthesis in a Lewis acidic medium, typically in $ZnCl_2$ salt melts. CTFs typically lack long-range order, yet display high porosities paired with exceptional chemical inertness and high thermal stability owing to their graphite-like composition and robust carbon–carbon and

carbon–nitrogen linkages.[17-18] The presence of well-defined binding sites inside the CTFs can bind and orient metal hydride nanoparticles and clusters, altering the electronic density distribution, for example, through Lewis donor-acceptor type interactions. We demonstrated that such interactions occur when $Mg(BH_4)_2$ is nanoconfined inside the pores of UiO-67(bipy),[15] however, in that particular case the presence of OH- in the Zr-oxo cluster leads to formation of stable B-O bonds. Aluminum is known to forms similarly strong Al-O bonds, therefore, we decided to focus on nominally oxygen-free CTF-biphenyl and CTF-bipyridine hosts.

Aluminum hydride AlH_3 was selected as the candidate hydride material as it has one of the highest hydrogen gravimetric capacity (10.1 wt%) and a volumetric hydrogen density twice that of liquid hydrogen (148 g H_2 L^{-1}).[19] However, AlH_3 is thermodynamically unstable (metastable) and only exists under ambient conditions because of kinetic stabilization.[20] Alane desorbs pure H_2 upon heating and forms metallic Al, however, to reform bulk AlH_3 from the metal, pressures in excess of 7,000 bar are required.[21-22] Through nanoconfinement the kinetics of H_2 release from AlH_3 can be accelerated, but reversibility still remains a problem.[23-24] Previous studies on bulk AlH_3 showed that the material can be rendered fully or almost fully reversible by formation of adducts with organic amines and ethers,[25-28] but complex regeneration schemes are required. Here, we show that confining AlH_3 inside a bipy-functionalized CTF enables reversible hydrogen uptake, with the dehydrogenated material displaying unprecedented reversibility as low as 700 bar H_2, more than 10 times lower compared to bulk aluminum.[21] A combination of advanced characterization and DFT calculations provide insights into the mechanism of thermodynamic stabilization and reversibility displayed by AlH_3@CTF-bipy, in which nanoclusters of AlH_3 pull electron density away from the nitrogen atoms of the bipyridine groups.

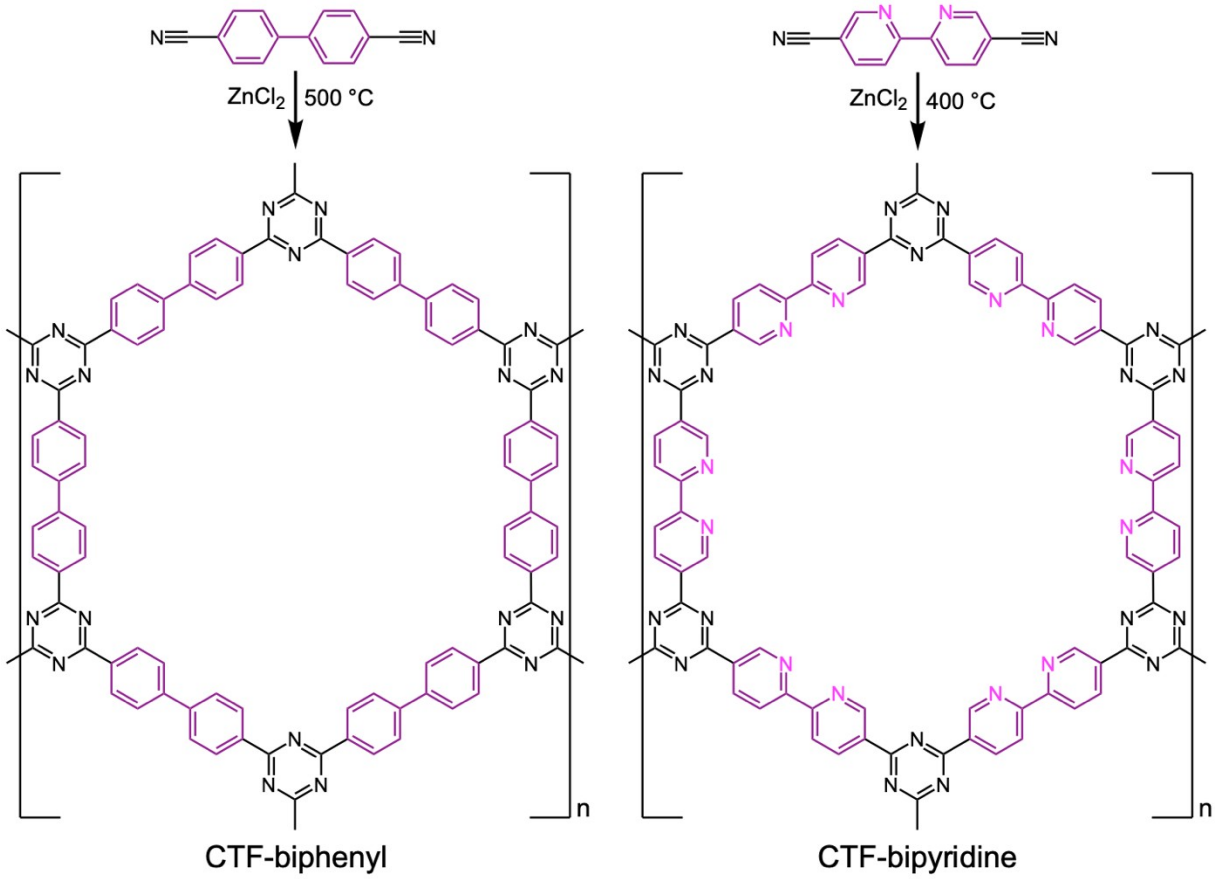

Scheme 1. The synthetic procedure for the biphenyl- and bipyridine-functionalized CTF materials.

Results and Discussion

CTF materials with two types of linkages were used as nanoconfinement scaffolds to probe the effect of pore functionalization on hydrogen storage properties of AlH_3: CTF-biphenyl (CTF-biph) and CTF-bipyridine (CTF-bipy) (**Scheme 1**). The two CTF hosts were synthesized via an ionothermal synthesis approach in anhydrous $ZnCl_2$ melt. The as-synthesized CTF materials were extensively washed with aqueous HCl, H_2O, tetrahydrofuran (THF), and acetone, then dried upon heating in vacuum (see **Supporting Information (SI)** for additional details). The XRD, FTIR, ^{1}H and ^{13}C MAS characterization of as-prepared CTF-biph and CTF-bipy materials is presented in **Figures S1** and **S2** (SI). The CTF scaffolds were heated to 250 °C under vacuum for 16 hours to remove possible adsorbed species from the pores prior to hydride infiltration. A commercially-

available solution of AlH_3 in dimethyl(ethyl)amine/toluene was used for infiltration into CTF-materials.[29] Alane is a white solid, however the color of the solvent-infiltrated samples was completely black without any precipitated white AlH_3 powder, suggesting that there was no bulk AlH_3 present. The residual amine and solvent can be removed by subjecting the infiltrated materials to dynamic vacuum for 72 hours with mild heating (up to 60 °C).

The XRD patterns of the as-activated CTF materials, and amine-free AlH_3@CTF-biph and AlH_3@CTF-bipy materials are shown in **Figure S3** (SI). The XRD patterns show broad features both before and after infiltration, which indicates a lack of long-range order in these materials. To track the distribution of AlH_3 species inside the CTF pores, we used Transmission Electron Microscopy (TEM) and Electron Energy Loss Spectroscopy (EELS), two techniques with appropriate space resolution for characterizing such materials. High-resolution TEM images show ~1.2 to 4.5 nm AlH_3 particles located throughout the amorphous CTF-biph and CTF-bipy hosts (Figure 1). The corresponding Al EELS signal was detected throughout the entire sample, implying that Al-containing species are located inside the pores, and do not exist as a separate phase. The average AlH_3 particle size for AlH_3@CTF-biph is 2.93 nm, while for AlH_3@CTF-bipy the average particle size is 1.82 nm (**Figure S4**, SI), consistent with hysteresis in the N_2 isotherms that indicate larger pores in CTF-biph, where larger hydride particles may agglomerate.

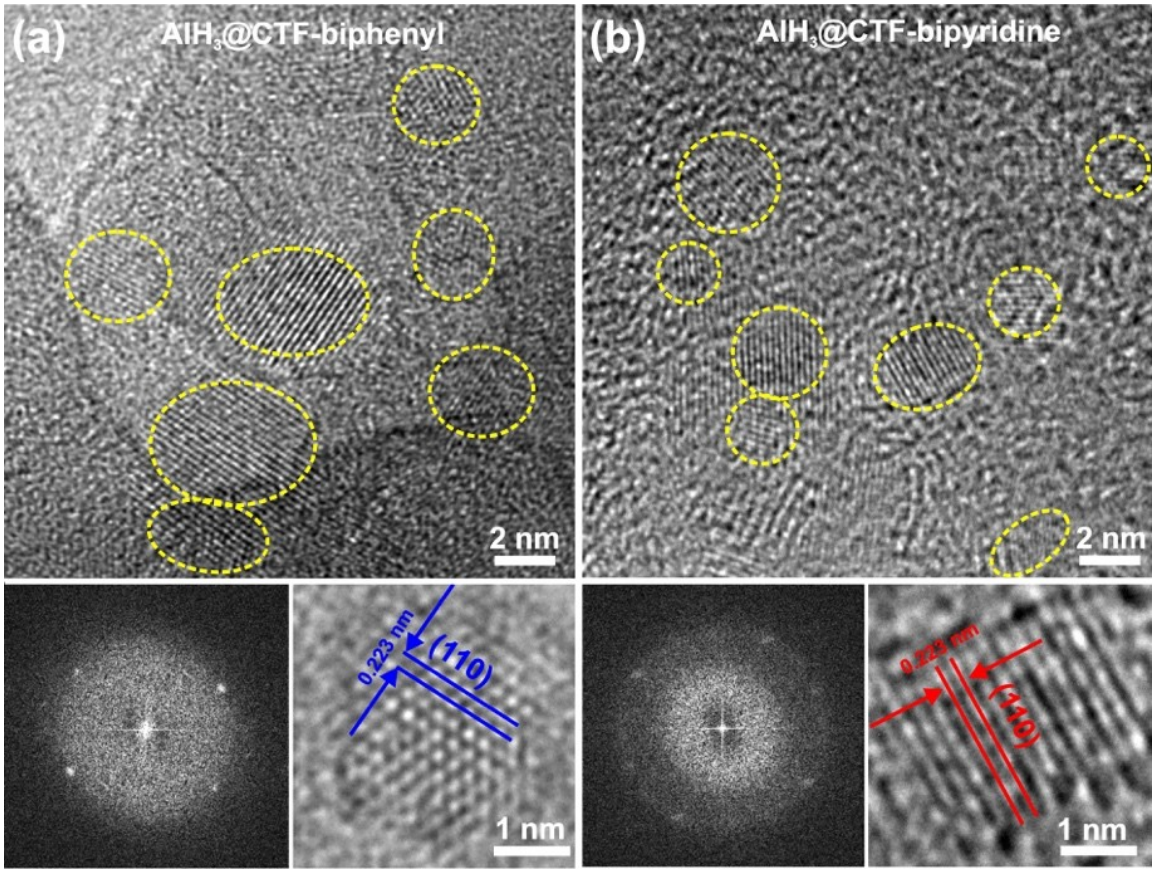

Figure 1. High-resolution TEM and electron diffraction data for AlH_3@CTF-biph and AlH_3@CTF-bipy. The observed d-spacings for the crystalline particles corresponds to γ-AlH_3.

Electron Energy Loss Spectroscopy (EELS) and X-ray photoelectron spectroscopy (XPS) provide useful information on the nature of chemical species and oxidation states. EELS spectra (**Figure 2a**) confirm the presence of spectral signatures of AlH_3,[30] as well as Al_2O_3 (likely from sample transfer to TEM chamber). The Al 2p XPS spectra of both materials could be fit by a single doublet, indicating that a single Al environment is present in the near surface region. The position of the Al $2p_{3/2}$ peak differs slightly between the two materials: 74.0 eV for AlH_3@CTF-biph and 73.6 eV for AlH_3@CTF-bipy; however, both are characteristic of AlH_3 species. This is based on our previous theoretical calculations which show that the 2p Al XPS binding energy changes in the following order Al-metal<Na_3AlH_6< AlH_3<$NaAlH_4$<Al_2O_3 ≈ $Al(OH)_3$, *i.e.* the more reduced Al species have lower XPS binding energies, whereas the more oxidized species have higher binding energies, with the aluminum-hydride binding energies in between.[31] The

literature reported values for the binding energy of metallic Al is 72.6 eV, whereas for Al_2O_3 this value is listed at 74.6 eV. The observed 0.4 eV shift (74.0 eV vs 73.6 eV) between the two samples reveals that electronic interactions between AlH_3 the CTF host differ in the two materials, with AlH_3 being more reduced in the CTF-bipy material.

Figure 2. (a) EELS data for AlH_3@CTF-biph and AlH_3@CTF-bipy. (b) Al 2p XPS data for AlH_3@CTF-biph and AlH_3@CTF-bipy showing AlH_3 species at 74.0 and 73.6 eV respectively. The raw data (grey dots), Al 2p doublet peak fit (filled peaks), and fit envelops (black lines) are shown. Spectra were calibrated using survey scans fit to the C-C peak at 284.8 eV.

Hydrogen desorption measurements were performed using the Sieverts (volumetric) method by heating the samples to release hydrogen and measuring the pressure increase with high-accuracy pressure transducers. The desorbed hydrogen storage capacity was calculated based on the total composite weight. The first cycle of hydrogen desorption, shown in **Figure 3(a)**, surprisingly revealed that the total hydrogen capacity of the AlH_3@CTF-bipy material is higher compared to that of AlH_3@CTF-biph (1.54 wt% for AlH_3@CTF-bipy vs 1.02 wt% for AlH_3@CTF-biph) even though the ratio of the surface areas for the two CTFs is 1.00:1.69 (1180 $m^2\ g^{-1}$ vs. 2000 $m^2\ g^{-1}$) and the ratio of pore volumes are 1.00:3.03 (1.91 $cm^3\ g^{-1}$ vs. 0.63 $cm^3\ g^{-1}$). This suggests that CTF-bipy has a higher affinity towards alane and facilitates higher hydride loading. If we assume AlH_3 is the only source of hydrogen, then the alane loading is calculated to be 15.6% by weight in AlH_3@CTF-bipy, and 10.1% by weight in AlH_3@CTF-biph. The nitrogen absorption isotherms at 77 K for the host and composite materials are shown in **Figure 3(b)**. As would be expected, the surface area and pore volume of the materials decrease upon AlH_3 infiltration. AlH_3@CTF-bipy has a surface area of 780 $m^2\ g^{-1}$ and a pore volume of 0.40 $cm^3\ g^{-1}$, while AlH_3@CTF-biph has a surface area of 1300 $m^2\ g^{-1}$ and a pore volume of 1.27 $cm^3\ g^{-1}$.

The initial rate of hydrogen release from both AlH_3@CTF-bipy and AlH_3@CTF-biph alane samples is extremely fast, with the onset dehydrogenation temperature of about 95 °C in both samples. Above 95 °C the dehydrogenation of both AlH_3@CTF-bipy and AlH_3@CTF-biph is fast, with ~2/3 of the total amount of hydrogen released within less than 10 minutes from the

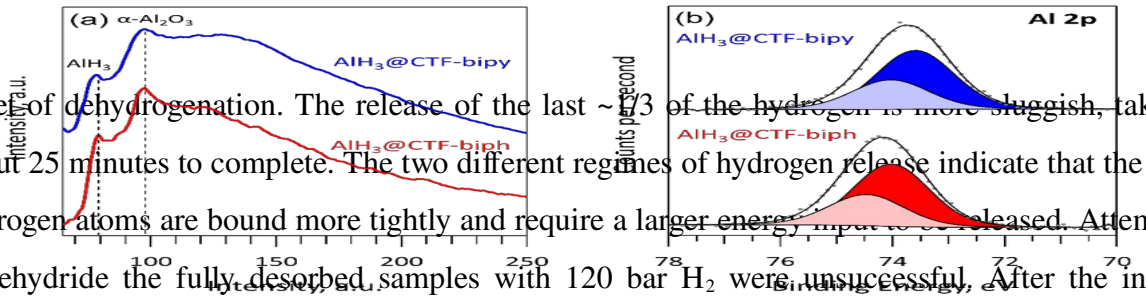

onset of dehydrogenation. The release of the last ~1/3 of the hydrogen is more sluggish, taking about 25 minutes to complete. The two different regimes of hydrogen release indicate that the last hydrogen atoms are bound more tightly and require a larger energy input to be released. Attempts to rehydride the fully desorbed samples with 120 bar H_2 were unsuccessful. After the initial dehydrogenation, the desorbed AlH_3@CTF-bipy and AlH_3@CTF-biph were exposed to 700 bar (70 MPa) hydrogen pressure in a custom stainless-steel reactor at 60 °C for 24 hours. After high-pressure hydrogenation, Sieverts measurements were performed on both samples, and a comparison between the 1st and 2nd H_2 desorption results is shown in **Figure 3(b)**. While the AlH_3@CTF-biph sample shows essentially no hydrogen being desorbed, remarkably, the cycled AlH_3@CTF-bipy material desorbs 0.65wt% hydrogen. This points out to significant thermodynamic changes, enabling direct rehydrogenation of aluminum species under conditions of pressure that are 70 times lower compared to bulk. For instance, Saitoh *et al*. hydrogenated bulk Al to trihydride at 8.9 GPa H_2 and 600 °C, while cycling reduces the pressure and temperature required for hydrogenation to 4.9 GPa and 330 °C.[21] *Ab initio* thermodynamic calculations of AlH_3 free energy by Graetz *et al*. indicate that hydrogenation should become favorable at pressures above 0.7 GPa (7,000 bar) at 27 °C, although experiments revealed that much higher pressures are required for this process.[22]

Figure 3. (a) Sieverts data for AlH_3@CTF-biph and AlH_3@CTF-bipy during the first and second cycle (1st and 2nd H_2 desorption). (b) Nitrogen absorption isotherms at 77 K for CTF-biph, AlH_3@CTF-biph, CTF-bipy, and AlH_3@CTF-bipy.

The small particle sizes due to nanoconfinement makes phase identification difficult especially if the particles are amorphous. Magic Angle Spinning Nuclear Magnetic Resonance (MAS NMR) is well suited for probing non-crystalline phases as it is sensitive to both species displaying long- and short-range order. In addition, the measured chemical shifts can be compared readily to chemical shifts from density functional theory (DFT) calculations, alleviating ambiguity in spectral interpretation. The aluminum speciation of the as-synthesized, desorbed, and rehydrogenated AlH_3@CTF-bipy samples are revealed with ^{27}Al MAS NMR and their spectra are shown in **Figure 4.** The spectra show a clear progression from hydrogen-rich Al

environments in the as-synthesized sample, to hydrogen deficient environments with formation of metallic Al, and then regeneration of Al-H species after rehydriding under 70 MPa (700 bar) H_2 pressure.

Surprisingly, the as-synthesized AlH_3@CTF-bipy sample does not display a single peak, but several Al chemical environments evident by the four distinct peaks between 130 and -35 ppm. These peaks are broadened by structural disorder from the high surface area of the aluminum hydride particles and many overlapping resonances resulting from Al being incorporated in varying cluster sizes and being complexed to the scaffold. However, the prominent two high frequency peaks are associated with tetrahedrally coordinated Al (Al^{IV}) species, while the lower frequency is similar to that observed for γ-AlH_3.[32] Tetrahedral Al is not expected from any of the bulk AlH_3 phases suggesting the presence of Al^{IV} is due to nanoconfinement effects to form small clusters and complexed Al as suggested by DFT and computational NMR calculations (see theory section below, **Table S1**, and **Figures S5-S7**, SI). Further experimental evidence that the tetrahedral Al at ~94 ppm is an aluminum hydride phase is from rotational-echo double resonance (REDOR) NMR, which acts as a filter to only show chemical environments with strong Al-H dipolar coupling interactions resulting from short interatomic distances. The REDOR NMR difference spectrum (**Figure S6**, SI) reveals two strong peaks at ~94 and 5.8 ppm. A small amount of amorphous Al_2O_3 (~10-15%) is also observed to contribute to the broadened peaks which formed during sample handling and transfer for the NMR measurement and can be observed in all spectra. After hydrogen desorption, the peaks assigned to alane phases essentially disappear and the spectrum is dominated by metallic Al species with a distinct chemical shift at 1639 ppm (**Figure 4**). [33] After desorption, small amounts of Al_2O_3 remain present, which is verified by the characteristic chemical shift and quadrupolar coupling constant of the two broadened peaks consistent with disordered γ-Al_2O_3.[34],[35]

The rehydrogenated AlH_3@CTF-bipy ^{27}Al MAS NMR spectrum shows the reappearance of tetrahedral Al-H clusters, confirmed by REDOR NMR (**Figures S6, S7**, SI), clearly demonstrating the regeneration of the hydride under relatively mild conditions at 700 bar H_2 and 60 °C. The rehydrogenated sample still displays metallic Al, indicating the alane regeneration is incomplete under these conditions. The presence of metallic Al was also confirmed with high-resolution TEM (**Figure S8**, SI). The minor intensity of the γ-AlH_3 phase relative to the Al-H

clusters indicates the latter are more energetically favorable and reversible during rehydrogenation. Integrating the area of the metallic Al and Al hydride regions across the spectra provides insight into the hydrogenation kinetic mechanisms (**Figure S7**, SI). Nearly 90% of Al-H phases in the as-synthesized AlH_3@CTF-bipy sample converts to metallic Al during desorption and around half of the metallic Al reforms Al-H clusters after rehydriding, in good agreement with the Sieverts data. This result indicates the Al-H clusters are the main contributor to reversible rehydrogenation.

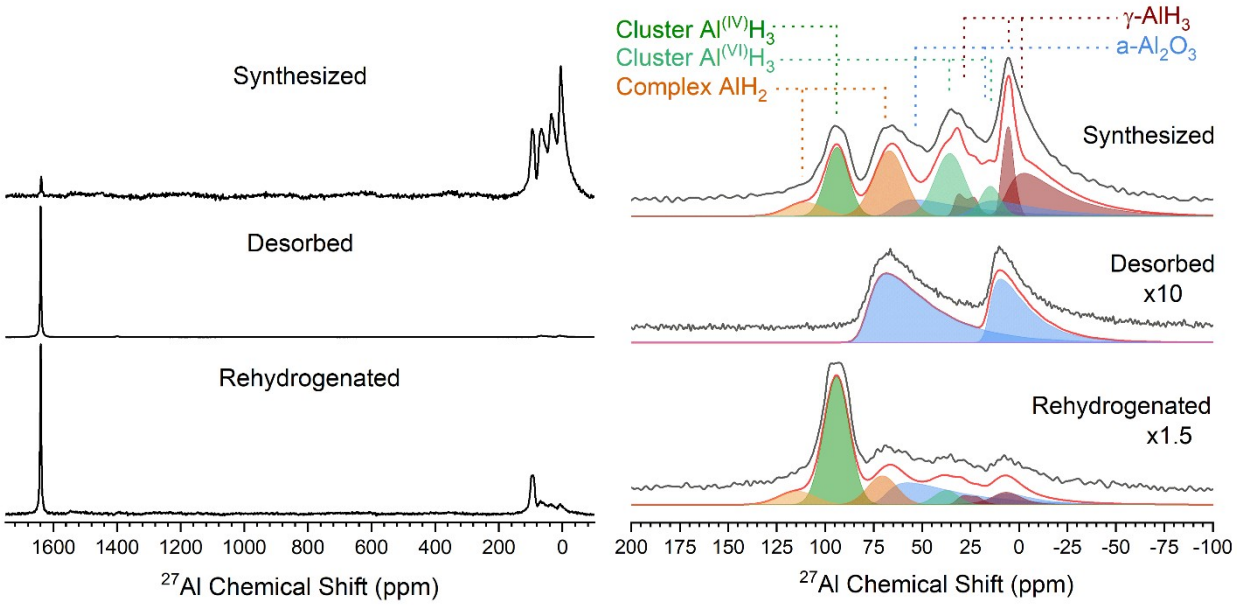

Figure 4. ^{27}Al MAS NMR spectra for the as-synthesized, desorbed, and rehydrogenated AlH_3@CTF-bipyridine. (left) Whole spectral range and (right) limited range of non-metallic Al species with a representative deconvolution including aluminum hydride clusters, complexed aluminium hydride, γ-AlH_3, and Al_2O_3. Peak intensity is scaled for the purposes of comparison.

MECHANISTIC UNDERSTANDING OF REVERSIBILITY

To explore the effect of confinement on the reversible hydrogen release and uptake, we generated cluster models of AlH_3 and Al with varying sizes to evaluate the reaction energy of hydrogenation (ΔE_{hyd}) at nanoscale. We sourced the global minimum structures of AlH_3 and Al clusters, ranging from one to eight formula units, and further optimized them with PBE-D3. DFT-computed ΔE_{hyd} values based on cluster models shown in **Figure 5a** are all lower

than the bulk ΔE_{hyd} (-6 kJ mol^{-1} H_2), but the difference narrows quickly with increasing cluster size. Vajeeston *et al.* observed a similar trend in DFT-computed ΔE_{hyd} for larger nanoparticle sizes and predicted a cut-off particle size of 1 nm where ΔE_{hyd} starts to resemble the bulk state value. Therefore, AlH_3 regeneration should be thermodynamically more favorable than the bulk phase reaction only if the small AlH_3 particles or clusters are enforced by tight spatial confinement at certain regions within the amorphous CTF host, partially rationalizing the observations that only a fraction of AlH_3 in the as-synthesized AlH_3@CTF-bipyridine were regenerated, and none could be regenerated in of CTF-biphenyl with a weaker confinement environment. To facilitate interpretation of the ^{27}Al MAS NMR spectra, we further computed the chemical shifts of individual Al atoms within each AlH_3 cluster using GIPAW method and linear regression parameters for a set of reference Al-containing bulk lattices (**Figure S9**, SI), and results shown in **Figure 5b**. Computed chemical shifts span a wide range, highlighting significant variations in local Al coordination environment within and across AlH_3 clusters. In general, chemical shifts below 40 ppm are associated with octahedral Al at/ near the center of clusters while those beyond 90 ppm are associated with tetrahedral Al at the corners. Notably, tetrahedral Al in the range between 90 and 100 ppm, corresponding the dominant peak observed for the rehydrogenated sample, have a common structural feature: sharing two hydrogen with one neighboring five-fold or octahedral Al (**Figure 10**, SI). The high tetrahedral to octahedral Al ratio (ratio of AlH_3 at the corner to those in the center of particles/clusters) in the rehydrogenated sample as observed in the ^{27}Al MASNMR spectrum clearly indicates that the regenerated AlH_3 are predominantly small clusters rich in tetrahedral sites.

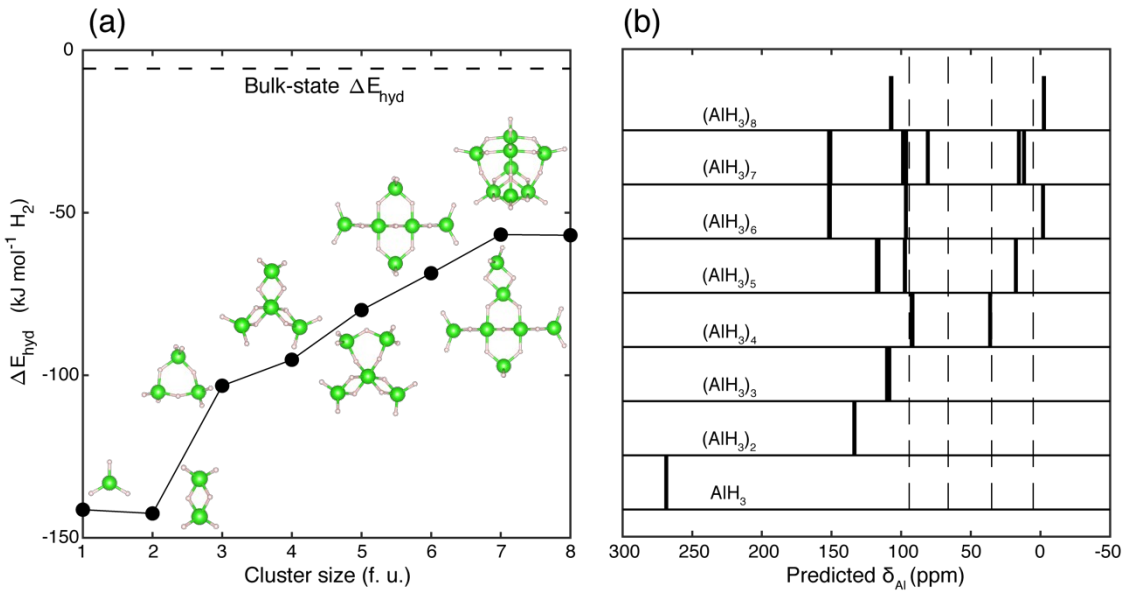

Figure 5. (a) DFT-computed 0-K reaction energies of Al -> AlH_3 hydrogenation based on bulk and cluster models. (b) Predicted isotropic chemical shifts of Al in AlH_3 cluster of varying sizes. Atom color: green – Al, pink – H. Dashed lines are experimental peak positions observed in Figure 4.

Another factor potentially influencing AlH_3 speciation and reversibility is the nature of chemical interactions between AlH_3 and the framework bipyridine sites in CTF-bipyridine. To probe such interactions, we constructed periodic CTF-bipyridine structures (**Figure S11**, SI) with/without molecular AlH_x (x = 0–3) units bonded to a bipyridine site. Based on the optimized structures, we computed the 0-K reaction energies of AlH_3 complexation, and subsequent stepwise release of H, plotted as a potential energy diagram in **Figure 6a**. Interestingly, the calculations indicate that AlH_3 can undergo dissociative adsorption to the CTF surface where one H in the molecular AlH_3 prefers to dissociate from Al and bond with a framework carbon bridging the bipyridine and triazine constituents (**Figures S12**, SI).

To relate the 0-K results in **Figure 6a** to conditions relevant to hydrogen adsorption/release, we computed Gibbs formation energies (G) of complexed AlH_x (x = 0–3) within the harmonic oscillator approximation (details described in **Supplementary note 1** of the **SI**). Computed phase diagram reporting the free-energy-minimizing species as a function of temperature (T) and H_2 partial pressure (P_{H2}) is shown in **Figure 6b**. Under hydrogenation condition (700 bars P_{H2} at 60

°C), the most stable species is complexed AlH_2 rather than AlH_3. In fact, complexed AlH_3 is never the preferred species under any conditions of interest, as partial dehydrogenation of complexed AlH_3 to AlH_2 is exothermic, and thus is bound to be exergonic by further including the entropic contribution associated with H release. Further dehydrogenation is plausible with elevated temperature and reduced P_{H2}: for instance, with low P_{H2} (10^{-6} bar), complexed AlH_2 is expected to be further dehydrogenated to AlH and Al at 150 and 230 °C, respectively. The computed Al chemical shift of the complexed AlH_2, 125 ppm as shown in **Figure 6c**, corresponds well with a tiny shoulder at around the same position in the ^{27}Al MAS NMR spectra, suggesting the existence of such species in both as-synthesized and rehydrogenated samples. Should the local pore environment allow, some complexed AlH_2 can potentially be bound by additional AlH_3 molecules or clusters, that may change their first-shell coordination and thus the Al chemical shifts of complexed AlH_2. To examine such scenarios, we modeled additional CTF-bipyridine structures by placing the AlH_3 molecule or clusters with varying sizes in close proximity with the pre-existing complexed AlH_2. DFT-optimized structures, included in **Figure 6c**, show that the first coordination shell of Al in complexed AlH_2 changes from tetrahedral to five-fold when tethered by additional AlH_3 species, resulting in smaller chemical shifts compared to the unbound complexed AlH_2. This partially accounts for the peak centered at around 70 ppm observed in the ^{27}Al MAS NMR spectra of as-synthesized and rehydrogenated samples.

The reversibility of bulk AlH_3 in the presence of a Lewis base can be achieved in the presence of amines and ethers using wet-chemistry and mechanochemical approaches, which in all cases leads to a significant reduction of the thermodynamic hydrogenation barrier of Al.[20, 36] This adduct approach enables the hydrogenation of Al at room temperature and reasonable pressures to generate AlH_3–ammine adducts, with full or almost full reversibility.[19, 25-28, 36] We show that similar interactions occur at nanoscale between AlH_3 and CTF-bipyridine, but not as strong between AlH_3 and CTF-biphenyl, as further DFT calculations (**Figure S13**, SI) indicate that the binding energy of AlH_3 to bipyridine site in CTF-bipy is about 1.5 eV lower than to the triazine site in CTF-biph. Thus, our experiments and calculations demonstrate that concomitant nanoconfinement and strong Lewis acid-base interactions can be successfully employed to tune the energetics of hydrogen release and uptake by metal hydrides.

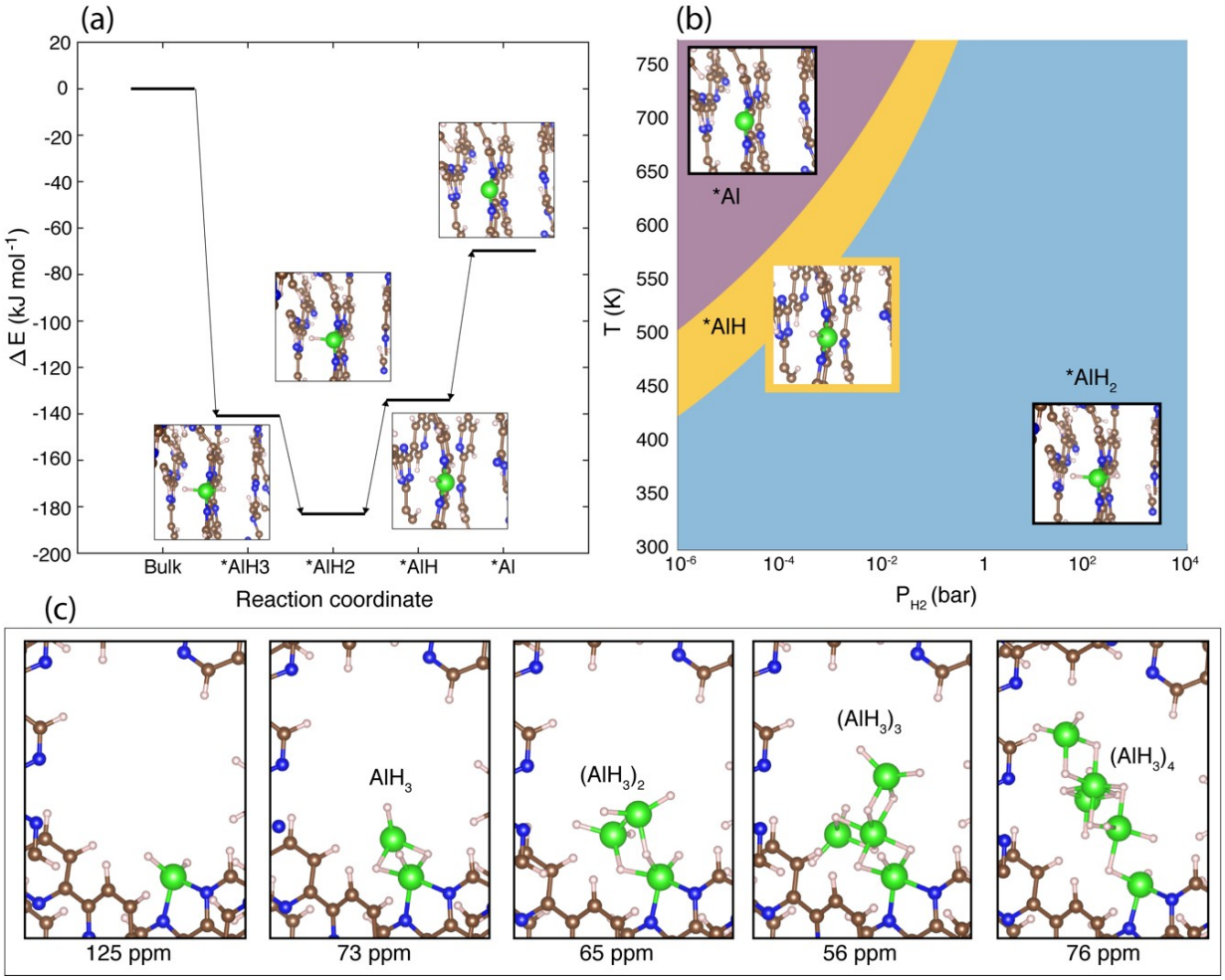

Figure 6. (a) DFT-computed potential energy diagram with zero-point energy corrections of AlH_3 complexation, and stepwise dehydrogenation. (b) Phase diagram of AlH_x speciation as a function of temperature (T) and H_2 partial pressure (P_{H2}). (c) DFT-optimized structures of complexed AlH_2 bound by $(AlH_3)_x$ (x = 0–4). Predicted Al chemical shifts of complexed AlH_2 are shown below each structure.

The ^{13}C cross polarization NMR of CTF-biph (**Figure S2c**, SI), with a peak at ca. 130 ppm is indicative of aromatic carbon. This and the low crystallinity indicated in the XRD pattern (**Figure S2a**, SI) suggest that CTF-biph may have regions of amorphous, locally graphitic, structure. We investigated alane-CTF binding energies by another set of calculations that approximates binding sites in CTF as defects in one monolayer locally graphitic carbon (graphene sheet). Details of the calculations are presented as **Supplementary note 2** in the **SI** (**Table S2**

and **Figure S14**). The results indicate that (1) graphene-like defects without N-heteroatoms will mostly react with and decompose AlH_3, which explain the observed irreversibility of AlH_3@CTF-biph, and (2) structurally small graphene-like defects with N-heteroatoms are too sterically constraining for Al in AlH_3 to fully access the N lone pairs *and* form stable clusters, implying that the area adjacent to pyridinic-N in CTF-bipy structure remains open enough for strong binding.

CONCLUSION

We demonstrate here a new strategy for thermodynamic stabilization of metal hydrides by incorporating alane clusters inside the pores of Covalent Triazine Frameworks. Small AlH_3 species are evenly distributed throughout the pores of CTF-bipyridine and CTF-biphenyl hosts upon solution infiltration. Although both frameworks can be loaded with alane, the presence of N bipyridine functionalities on CTF-bipy enables significant electron transfer between the host and the hydride. DFT calculations and computational spectroscopy were used to assign the complex ^{27}Al MAS NMR chemical shifts which span between -35 to 130 ppm, highlighting significant variations in local Al coordination environment in AlH_3 clusters. The AlH_3@CTF-bipyridine and AlH_3@CTF-biphenyl samples start desorbing hydrogen as low as 90-95 °C. Above 95 °C the dehydrogenation is very fast, with ~2/3 of the total amount of hydrogen released within less than 10 minutes from the onset of dehydrogenation. The AlH_3@CTF-bipy material can be rehydrogenated at 70 MPa (700 bar) H_2, as clearly demonstrated by Sieverts, ^{27}Al MAS and ^{27}Al{^{1}H} REDOR NMR experiments. In bulk aluminum, hydrogenation can only occur at 7,000 bar H_2 and above.[21-22] Remarkably, no reversibility was observed for the AlH_3@CTF-biphenyl material, which supports the hypothesis that strong Lewis base bipyridine groups are critical to enabling reversibility in AlH_3.[19-20, 25-27, 37]

Our modeling results suggest that maintaining small alane cluster size, coupled with efficient electron density redistribution between the bipyridine groups and hydride is critical to the observed reversibility. The strategy of thermodynamic stabilization through concomitant nanoconfinement and host-guest electron transfer we introduce here could enable reversibility in other high-capacity metastable metal hydrides, such as ammonia borane, metal amidoboranes,

and $LiAlH_4$.[38-40] In addition, many other MOF and COF hosts exist that can provide precise control over the orientation of hydride clusters, and display a high density of Lewis base groups. Such groups could provide a higher degree of thermodynamic stabilization, which could in turn enable full hydride reversibility near ambient conditions. In a broader context, we envision a wide range of uses for "thermodynamic stability tuning" of small nanoparticles or clusters confined within suitable host materials to address emerging challenges in the area of energy generation and storage.

ASSOCIATED CONTENT

Supporting Information. Additional calculations, experimental details, and XRD, MAS NMR, FTIR, and TEM data.

AUTHOR INFORMATION

Corresponding Authors

Vitalie Stavila (vnstavi@sandia.gov); Mark D. Allendorf (mdallen@sandia.gov).

ACKNOWLEDGMENTS

We thank Brandan Davis and Robert Horton for their assistance with hydrogen uptake and release experiments. We also thank C. Minke for solid-state NMR measurements on as-synthesized CTF materials. Sandia National Laboratories is a multimission laboratory managed and operated by National Technology and Engineering Solutions of Sandia, LLC., a wholly owned subsidiary of Honeywell International, Inc., for the U.S. Department of Energy's National Nuclear Security Administration under contract DE-NA-0003525. The authors gratefully acknowledge funding from the U.S. Department of Energy, Office of Energy Efficiency and Renewable Energy, Fuel Cell Technologies Office, through the Hydrogen Storage Materials Advanced Research Consortium (HyMARC). The computational portion of the work was performed under the auspices of the DOE by Lawrence Livermore National Laboratory (LLNL) under Contract DE-AC52-07NA27344, with computing support from the LLNL Institutional

Computing Grand Challenge program. This work was supported by the Laboratory Directed Research and Development (LDRD) program at Sandia National Laboratories. Any subjective views or opinions that might be expressed in the paper do not necessarily represent the views of the U.S. Department of Energy or the United States Government. Funding is gratefully acknowledged from the ERC Starting Grant (project COFLeaf, grant number 639233).

Conflict of interest. The authors declare no conflict of interest.

KEYWORDS*: Nanoconfinement, Metal Hydrides, Covalent Triazine Frameworks, Hydrogen Storage, Coordination Chemistry.*

References:

[1] *Road Map to a US Hydrogen Economy*, http://www.fchea.org/us-hydrogen-study, Washington DC, USA, **2020**.

[2] *Germany's National Hydrogen Strategy*, https://www.bmwi.de/Redaktion/EN/Publikationen/Energie/the-national-hydrogen-strategy.html, Berlin, Germany, **2020**.

[3] R. Moradi, K. M. Groth, *International Journal of Hydrogen Energy* **2019**, *44*, 12254-12269.

[4] X. Liu, G. S. McGrady, H. W. Langmi, C. M. Jensen, *Journal of the American Chemical Society* **2009**, *131*, 5032-5033.

[5] J. Graetz, J. Wegrzyn, J. J. Reilly, *Journal of the American Chemical Society* **2008**, *130*, 17790-17794.

[6] A. Schneemann, J. L. White, S. Kang, S. Jeong, L. F. Wan, E. S. Cho, T. W. Heo, D. Prendergast, J. J. Urban, B. C. Wood, M. D. Allendorf, V. Stavila, *Chemical Reviews* **2018**, *118*, 10775-10839.

[7] V. Stavila, R. K. Bhakta, T. M. Alam, E. H. Majzoub, M. D. Allendorf, *ACS Nano* **2012**, *6*, 9807-9817.

[8] A. Schneemann, J. L. White, S. Kang, S. Jeong, L. W. F. Wan, E. S. Cho, T. W. Heo, D. Prendergast, J. J. Urban, B. C. Wood, M. D. Allendorf, V. Stavila, *Chemical Reviews* **2018**, *118*, 10775-10839.

[9] C. L. Carr, W. Jayawardana, H. Zou, J. L. White, F. El Gabaly, M. S. Conradi, V. Stavila, M. D. Allendorf, E. H. Majzoub, *Chemistry of Materials* **2018**, *30*, 2930-2938.

[10] C. L. Carr, E. H. Majzoub, *The Journal of Physical Chemistry C* **2016**, *120*, 11426-11432.

[11] S. J. Lyle, P. J. Waller, O. M. Yaghi, *Trends in Chemistry* **2019**, *1*, 172-184.

[12] H. Furukawa, K. E. Cordova, M. O'Keeffe, O. M. Yaghi, *Science* **2013**, *341*, 974-+.

[13] M. Kalaj, S. M. Cohen, *ACS Central Science* **2020**, *6*, 1046-1057.

[14] A. Rossin, G. Tuci, L. Luconi, G. Giambastiani, *Acs Catalysis* **2017**, *7*, 5035-5045.

[15] A. Schneemann, L. F. Wan, A. S. Lipton, Y. S. Liu, J. L. Snider, A. A. Baker, J. D. Sugar, C. D. Spataru, J. H. Guo, T. S. Autrey, M. Jorgensen, T. R. Jensen, B. C. Wood, M. D. Allendorf, V. Stavila, *ACS Nano* **2020**, *14*, 10294-10304.

[16] Y. J. Wu, C. Y. Wang, *Acs Sustainable Chemistry & Engineering* **2019**, *7*, 16013-16025.

[17] P. Kuhn, M. Antonietti, A. Thomas, *Angewandte Chemie International Edition* **2008**, *47*, 3450-3453.

[18] P. Kuhn, A. Thomas, M. Antonietti, *Macromolecules* **2009**, *42*, 319-326.

[19] B. M. Wong, D. Lacina, I. M. B. Nielsen, J. Graetz, M. D. Allendorf, *Journal of Physical Chemistry C* **2011**, *115*, 7778-7786.

[20] J. Graetz, B. C. Hauback, *MRS Bull.* **2013**, *38*, 473-479.

[21] H. Saitoh, A. Machida, Y. Katayama, K. Aoki, *Applied Physics Letters* **2008**, *93*, 151918.

[22] J. Graetz, S. Chaudhuri, Y. Lee, T. Vogt, J. T. Muckerman, J. J. Reilly, *Physical Review B* **2006**, *74*, 214114.

[23] P. K. Prabhakaran, L. Catoire, J. Deschamps, *Microporous and Mesoporous Materials* **2017**, *243*, 214-220.

[24] L. Wang, A. Rawal, K. F. Aguey-Zinsou, *Chemical Engineering Science* **2019**, *194*, 64-70.

[25] J. Graetz, S. Chaudhuri, J. Wegrzyn, Y. Celebi, J. R. Johnson, W. Zhou, J. J. Reilly, *Journal of Physical Chemistry C* **2007**, *111*, 19148-19152.

[26] D. Lacina, J. Wegrzyn, J. Reilly, Y. Celebi, J. Graetz, *Energy & Environmental Science* **2010**, *3*, 1099-1105.

[27] C. B. Ni, L. Yang, J. T. Muckerman, J. Graetz, *Journal of Physical Chemistry C* **2013**, *117*, 2628-2634.

[28] L. Sandig-Predzymirska, J. Ortmeyer, J. Wagler, E. Brendler, F. Habermann, M. Anders, M. Felderhoff, F. Mertens, *Dalton Transactions* **2020**, *49*, 17689-17698.

[29] E. Ashby, G. Brendel, H. Redman, *Inorganic Chemistry* **1963**, *2*, 499-504.

[30] S. Muto, K. Tatsumi, K. Ikeda, S. Orimo, *Journal of Applied Physics* **2009**, *105*, 123514.

[31] J. L. White, A. J. E. Rowberg, L. F. Wan, S. Kang, T. Ogitsu, R. D. Kolasinski, J. A. Whaley, A. A. Baker, J. R. I. Lee, Y.-S. Liu, L. Trotochaud, J. Guo, V. Stavila, D. Prendergast, H. Bluhm, M. D. Allendorf, B. C. Wood, F. El Gabaly, *ACS Applied Materials & Interfaces* **2019**, *11*, 4930-4941.

[32] S.-J. Hwang, R. C. Bowman, J. Graetz, J. J. Reilly, W. Langley, C. M. Jensen, *Journal of Alloys and Compounds* **2007**, *446-447*, 290-295.

[33] V. P. Tarasov, G. A. Kirakosyan, *Russian Journal of Inorganic Chemistry* **2008**, *53*, 2048-2081.

[34] A. R. Ferreira, E. Küçükbenli, A. A. Leitão, S. de Gironcoli, *Physical Review B* **2011**, *84*, 235119.

[35] S. K. Lee, S. B. Lee, S. Y. Park, Y. S. Yi, C. W. Ahn, *Physical Review Letters* **2009**, *103*, 095501.

[36] J. Ortmeyer, A. Bodach, L. Sandig-Predzymirska, B. Zibrowius, F. Mertens, M. Felderhoff, *ChemPhysChem* **2019**, *20*, 1360-1368.

[37] J. Graetz, J. J. Reilly, V. A. Yartys, J. P. Maehlen, B. M. Bulychev, V. E. Antonov, B. P. Tarasov, I. E. Gabis, *Journal of Alloys and Compounds* **2011**, *509*, S517-S528.

[38] Y. R. Zhao, M. Han, H. X. Wang, C. C. Chen, J. Chen, *Inorg. Chem. Front.* **2016**, *3*, 1536-1542.

[39] L. Wang, A. Rawal, M. Z. Quadir, K. F. Aguey-Zinsou, *Int. J. Hydrogen Energy* **2017**, *42*, 14144-14153.

[40] P. Ngene, M. H. W. Verkuijlen, C. Barre, A. P. M. Kentgens, P. E. de Jongh, *Nano Energy* **2016**, *22*, 169-178.